PNAS
www.pnas.org

Supplementary Information for

Direct observation of individual tubulin dimers binding to growing microtubules

Keith J. Mickolajczyk[1,2], Elisabeth A. Geyer[3,4,5], Tae Kim[3,4,5], Luke M. Rice[3,4*], and William O. Hancock[1,2*]

[1]Department of Biomedical Engineering, Penn State University, University Park, Pennsylvania, USA.
[2]Intercollege Graduate Degree Program in Bioengineering, Penn State University, University Park, Pennsylvania, USA.
[3]Department of Biophysics, University of Texas Southwestern Medical Center, Dallas, TX
[4]Department of Biochemistry, University of Texas Southwestern Medical Center, Dallas, TX
[5]These authors provided equal contributions

*** Corresponding Authors:**
William O. Hancock
Email: wohbio@engr.psu.edu

Luke M. Rice
Email: luke.rice@UTSouthwestern.edu

This PDF file includes:

Figs. S1 to S9
Captions for movies S1 to S3
References for SI reference citations

Other supplementary materials for this manuscript include the following:

Movies S1 to S3

www.pnas.org/cgi/doi/10.1073/pnas.1815823116

Supplemental figures

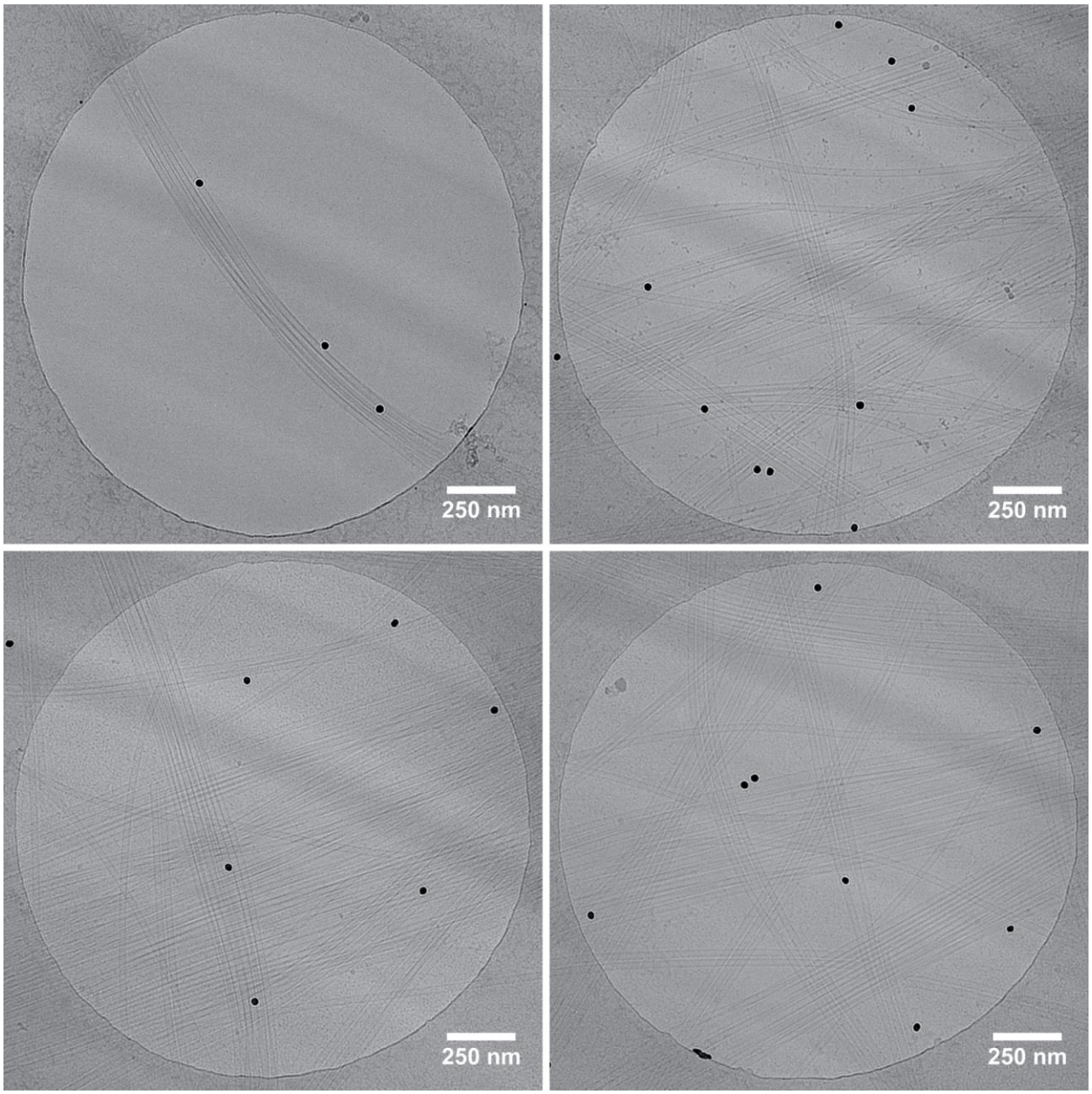

Fig. S1. Cryo-electron microscopy images of gold-labeled tubulin within microtubules. Biotinylated Tub2-KCK was pre-mixed with streptavidin-coated 20-nm gold nanoparticles at a 1000:1 stoichiometry and polymerized in solution. Gold-tubulin was observed to have polymerized into microtubules at multiple different protofilament positions and was seen to have not induced local defects.

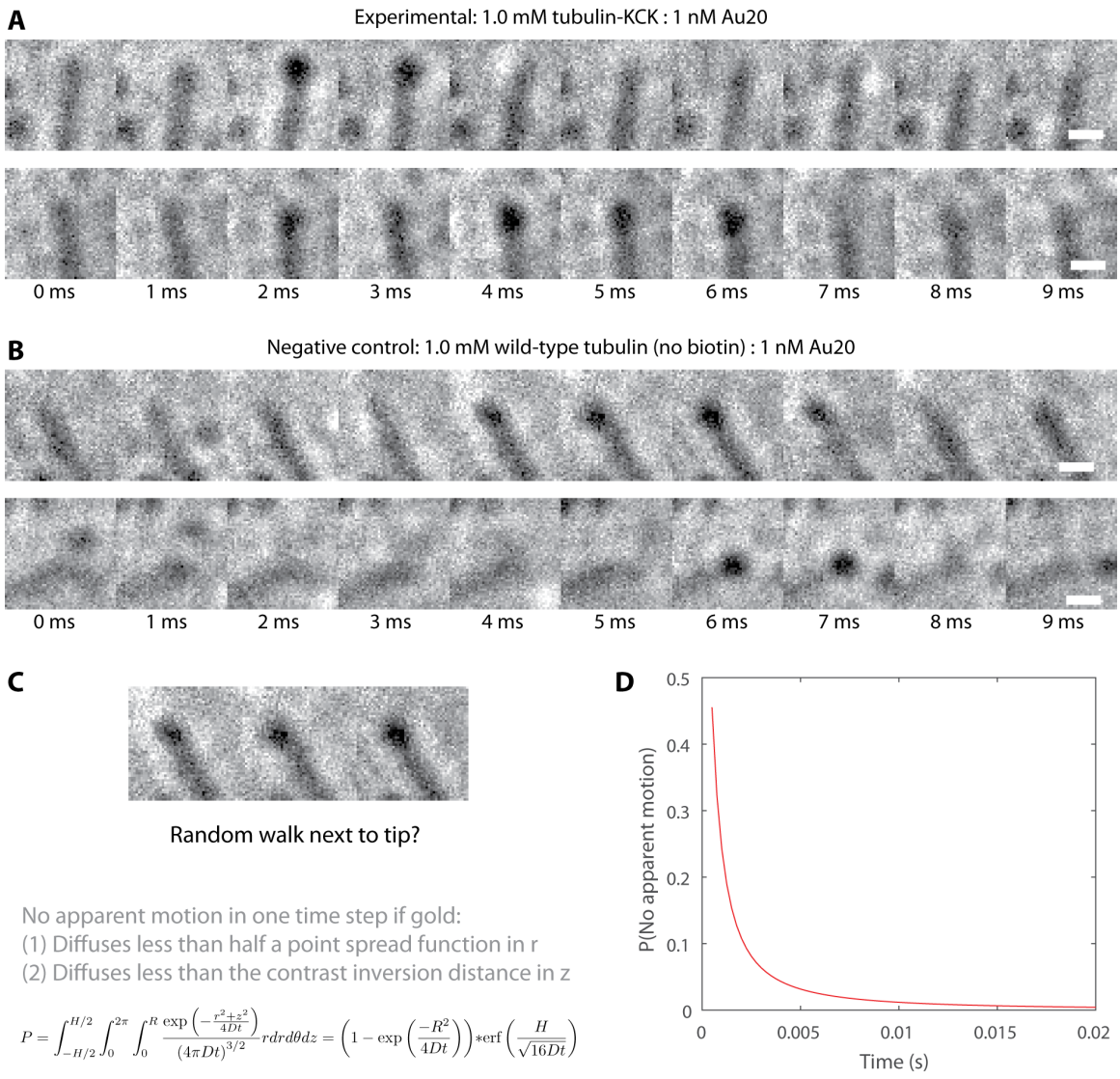

Fig. S2. At very high frame rates, gold diffusion and gold-tubulin reversible binding are ambiguous. (A) Apparent tip binding events at 1,000 frames per second (900 μs exposure) with 1 μM tubulin-KCK and 1 nM gold. **(B)** Apparent tip binding events at 1,000 frames per second with 1 μM wild-type tubulin and 1 nM gold. Wild-type tubulin is not biotinylated and cannot attach to the gold. Hence, these apparent events are false positives. **(C)** At short time steps, the gold may just be diffusing near the tip and, by chance, not move far enough away to move the apparent point spread function (PSF). Conservatively, the PSF would appear stationary within the image plane if the gold failed to move one PSF radius (R) away. In iSCAT, the color of the gold would invert from black to white if it were to diffuse in Z, with a complete inversion occurring at a distance H/2, approximately one sixth of a wavelength(12). The probability of a random walk not escaping these bounds is defined by a Gaussian distribution(13). **(D)** The probability of diffusing gold (diffusion constant $D=2.78*10^7$ nm^2-s^{-1} at 30° C) appearing like tip-bound gold as a function of time step. The results indicate that apparent events much shorter than 10 ms may simply be diffusion, and that false positives of 20 ms and longer are highly unlikely.

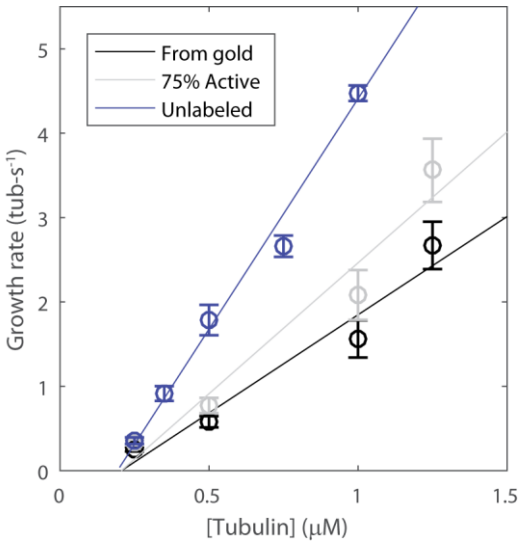

Fig. S3. Microtubule growth rate determined by individual tubulin landing events. (Black) the number of tubulins added to growing microtubule tips per second, calculated by dividing the number of observed irreversible gold-tubulin binding events per second (Fig. 2) by the ratio of labeled to unlabeled tubulins. (Gray) The growth rate determined by the gold-tubulin irreversible binding rate with a correction factor assuming 25% of the gold is lost to nonspecific surface binding (Fig. 1E). (Blue) The microtubule growth rate determined by microtubule length change over time (replicated from Fig. 1D), converted from nm per second to tubulins per second by multiplying by 13 protofilaments and dividing by 8 nm (length of one tubulin). The close agreement of these curves indicates that gold-tubulin binding events are proper representations of unlabeled tubulin binding events.

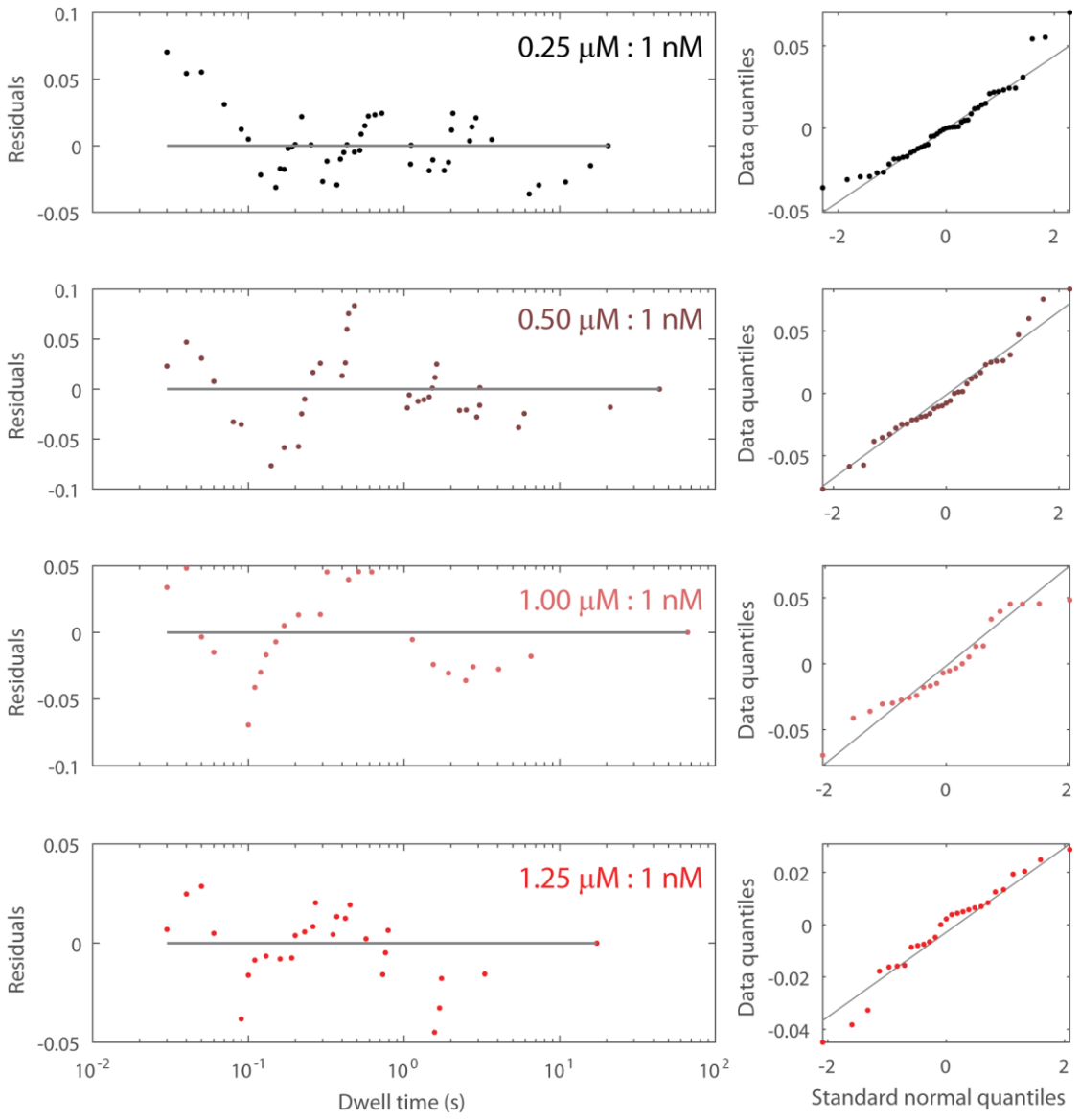

Fig. S4. Residuals from biexponential fitting to off-rate data. Data correspond to the fits shown in Fig. 3. Linear trends in the normality tests (right column) show that the residuals are normally distributed and indicate the quality of the fits. Stated ratios are of biotinylated tubulin-KCK to streptavidin-coated 20-nm gold nanoparticles.

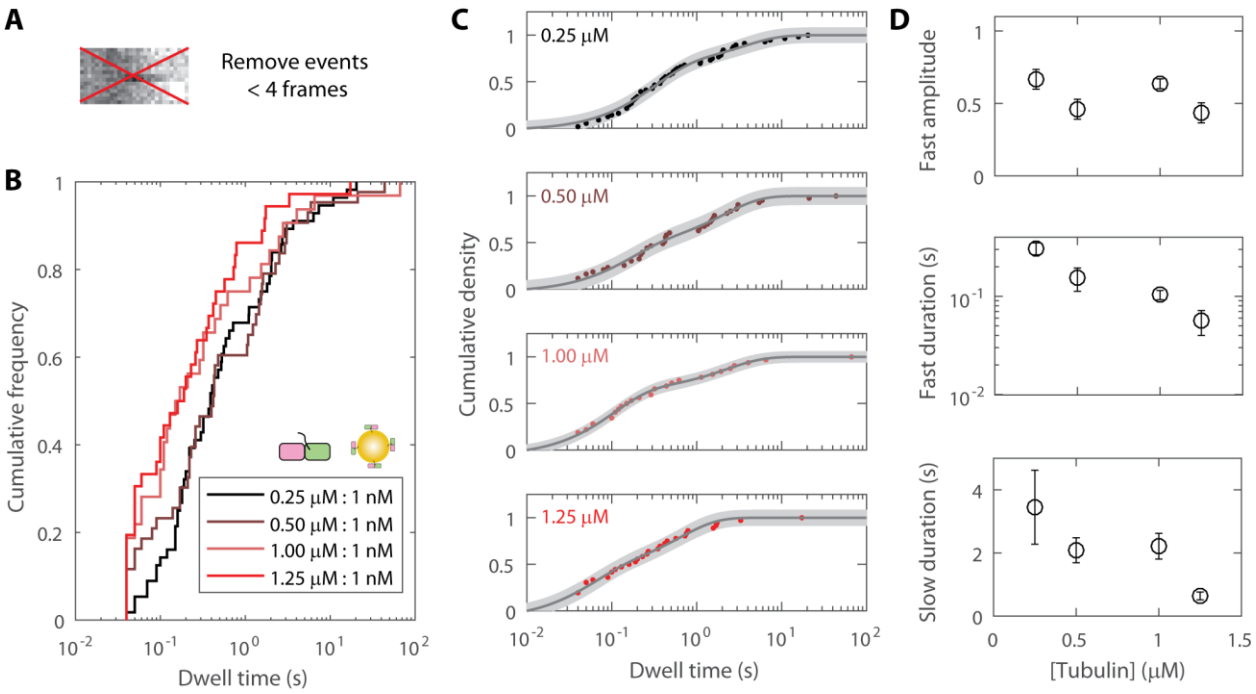

Fig. S5. Tubulin reversible dwell time analysis with a 40 ms cutoff. (A) The reversible dwell events for Fig. 3 were re-analyzed with the most frequent events (20 and 30 ms) removed. **(B)** Dwell time distributions with 20 and 30 ms events removed (N=56, N=43, N=32, and N=36 for 0.25, 0.50, 1.00, and 1.25 µM, respectively). The shapes of the distributions flattened, but the trend of lower free-tubulin concentrations having longer dwells remained. **(C)** Biexponential fits to the data in (B), with uncertainty in the fit shown as a gray region. **(D)** Fitted parameters from (C) show the same trend as the entire data set (Fig. 3D), with the fraction of fast events remaining constant but fast and slow phase characteristic dwell times decreasing substantially with increasing free-tubulin. Overall, this analysis shows that the free-tubulin dependence of the observed off-rate is not dominated by very short events, or by shifting weight between the two phases.

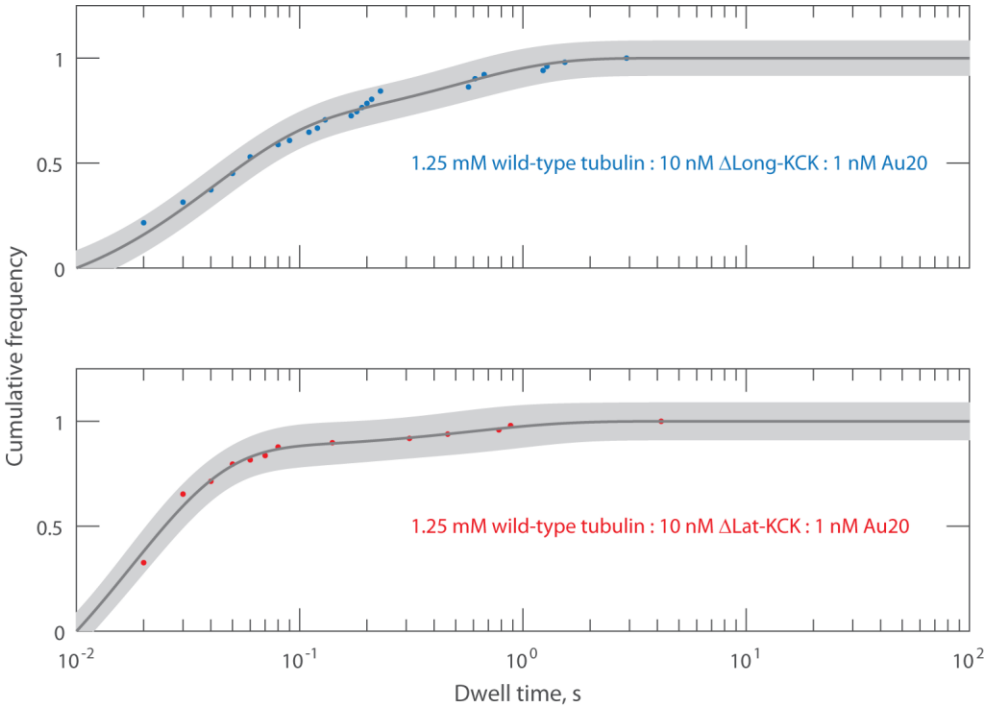

Fig. S6. Fits to mutant tubulin dwell time distributions. Fits for mutant tubulin dwell time distributions are shown in Figure 4E of the main text.

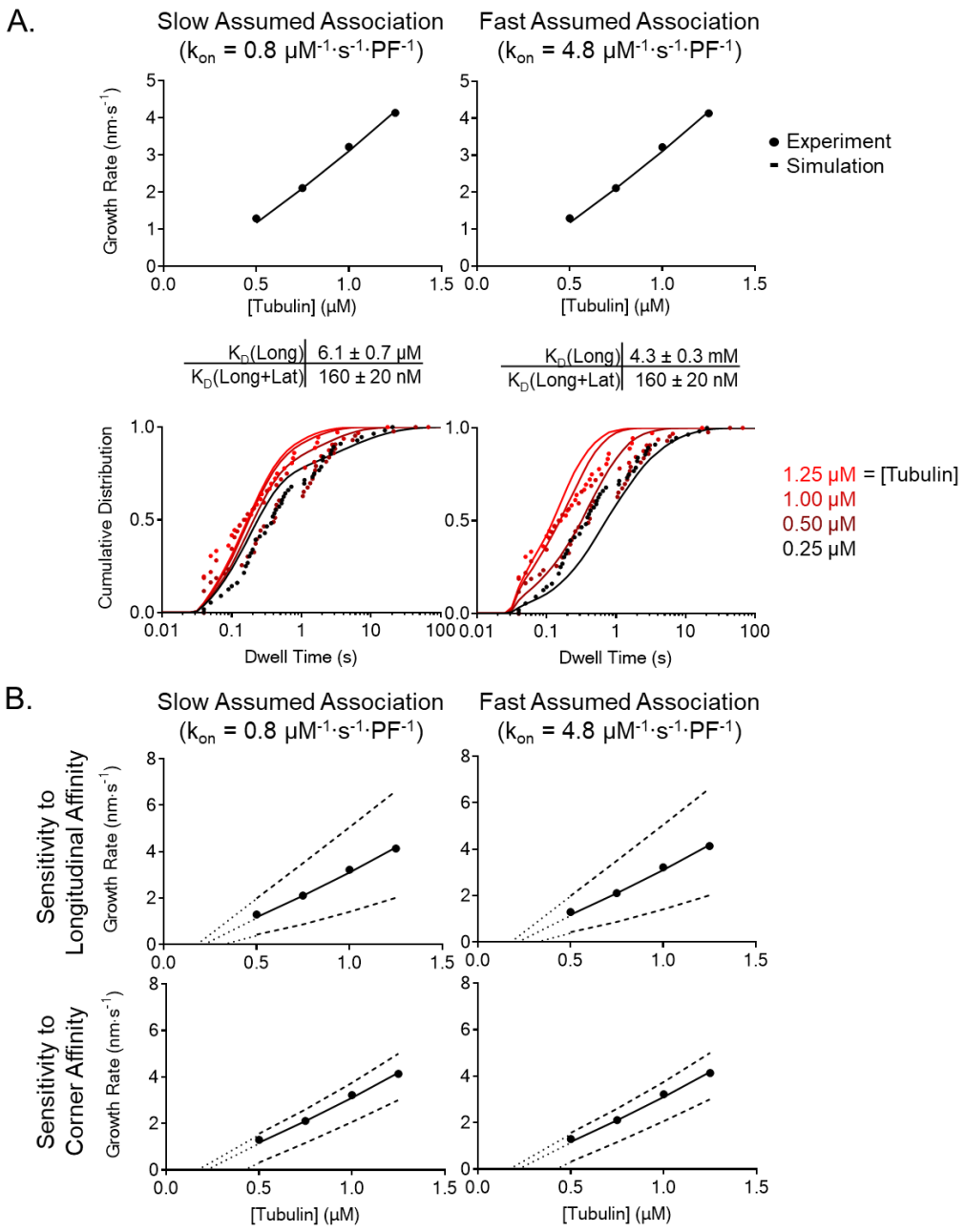

Fig. S7. Fitting models to the experimental data. (A) Model parameters (affinity of longitudinal and longitudinal+lateral interactions) for an assumed k_{On} were determined by fitting simulated growth rates and dwell times to the measured values. Inset shows the fitted parameters. **(B)** Sensitivity of growth rates to variations in the two model parameters. Top panels: Dashed lines show that increasing/decreasing longitudinal affinity two-fold affects the concentration-dependence (slope) of MT growth of rates; this slope is related to the apparent on-rate constant. Bottom panels: Dashed lines show that increasing/decreasing longitudinal+lateral affinity two-fold affects the x-intercept, but not the slope, for MT growth; the x-intercept is related to the apparent equilibrium constant for elongation.

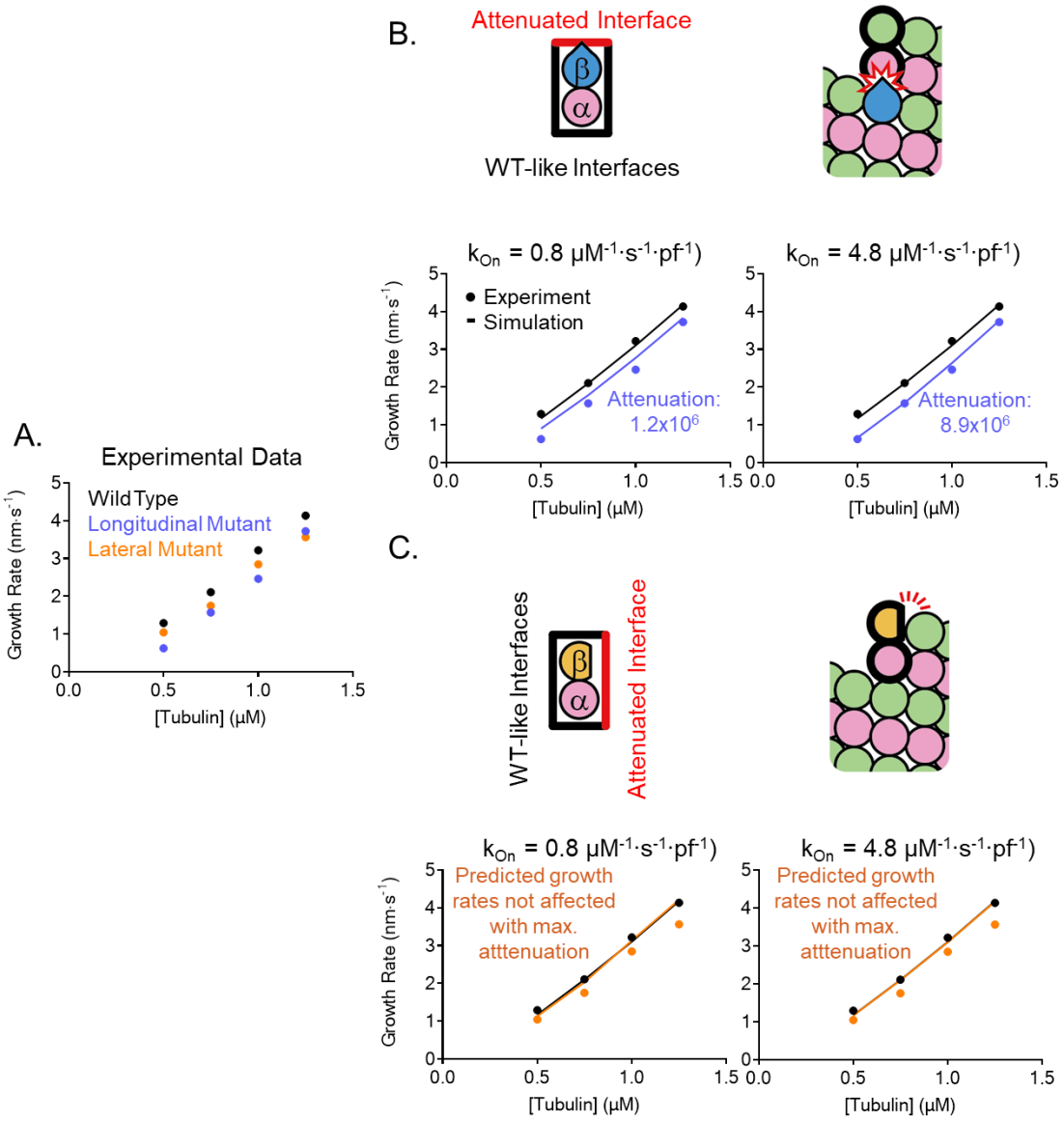

Fig. S8. Fitting the mutant simulation models to the experimental data. (A) Measured growth rates for wild-type (WT) MTs (black), WT MTs with 10nM ΔLong-tubulin (β: T175R, V179R mutations, blue), and WT MTs with 10nM ΔLat-tubulin (β:F281A mutation, orange). Data are reproduced from Fig. 4. **(B)** Cartoon illustrating how in simulations with ΔLong-tubulin, longitudinal interactions involving the plus-end of the mutant are attenuated (red edge of the box representing the interfaces within a MT lattice), while the other interfaces are unaffected (black). Attenuation factors for a given k_{On} are determined by fitting the model predictions to the experimental values on the growth rates of MTs containing longitudinal mutants. Inset: fitted longitudinal attenuation factors. **(C)** Cartoon illustrating how in simulations with ΔLat-tubulin, lateral interactions involving the right side (viewed from the outside of the MT) of the mutant are attenuated (red), while the other interfaces are unaffected (black). Even with maximal attenuation (i.e. cancelling the contribution of the lateral interface), the model could not reproduce the observed decrease in growth rate. More complex models may be required to capture the effects of this mutation.

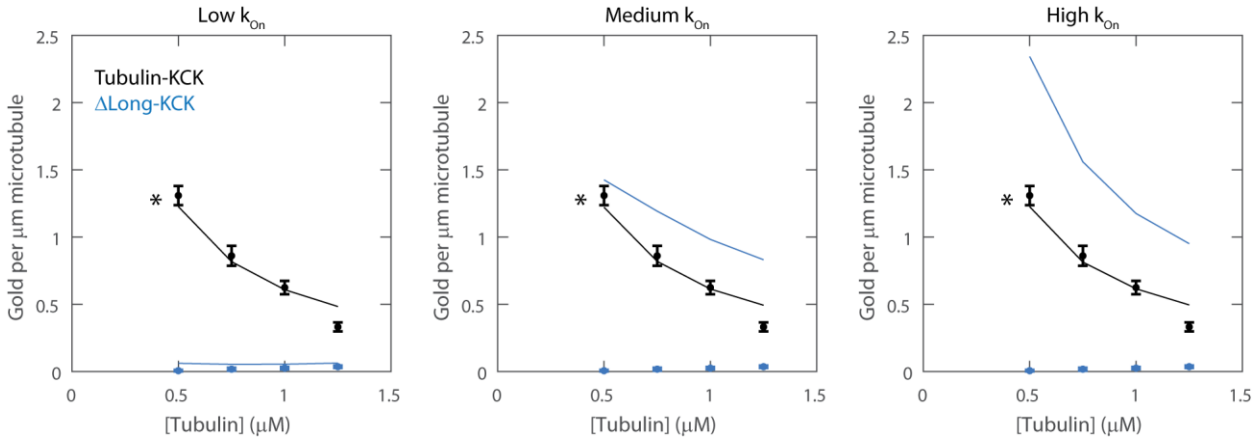

Fig. S9. Experimental and simulated gold per micron at all tubulin concentrations. Experimental data are shown as mean ± SEM for four tubulin concentrations (replicated from Fig. 4C). Simulated data from the computational model (with a 0.75x correction factor, Fig. 1D) run at three different tubulin k_{On} values (10.4, 31.2, and 62.4 $\mu M^{-1}s^{-1}tip^{-1}$) are shown as lines. Asterisk denotes that only half as much gold was used in the tubulin-KCK experiment versus the mutant. For wild-type tubulin-KCK (black), simulated gold per micron matched experimental values across a range of tubulin k_{On} values. For the ΔLong-KCK mutant (blue), simulations using a low tubulin k_{On} value matched the experimental, whereas simulations using a larger k_{On} values led to significantly more predicted gold per micron than observed experimentally. Thus, the ΔLong-KCK data rule out models having tubulin k_{On} values substantially above 10 $\mu M^{-1}s^{-1}tip^{-1}$.

Supplemental figure captions

Movie S1.

Example movie of growth assay with 1.0 μM Tub2-KCK and 0.5 nM of 20-nm gold nanoparticles present (2 frames per second). Gold-Tub2-KCK can occasionally be seen incorporating into growing microtubule tips. Microtubules (unlabeled) continue to grow after gold-Tub2-KCK incorporation. Notably, new gold only appears at growing microtubule tips. Scale bar 2.5 μm.

Movie S2.

Example movie of a reversible gold-Tub2-KCK binding event (100 frames per second). Scale bar 0.5 μm.

Movie S3

Example movie of an irreversible gold-Tub2-KCK binding event (100 frames per second). The microtubule shows thermal fluctuations, and the gold-Tub2-KCK fluctuates with it. Scale bar 0.5 μm.

References

1. Andrecka J, et al. (2015) Structural dynamics of myosin 5 during processive motion revealed by interferometric scattering microscopy. *Elife* 4:e05413.
2. Berg HC (1993) *Random Walks in Biology* (Princeton University Press).